

Nigel - Mechatronic Design and Robust Sim2Real Control of an Over-Actuated Autonomous Vehicle

Chinmay V. Samak* , Tanmay V. Samak* , Javad M. Velni and Venkat N. Krovi

Abstract—Simulation to reality (sim2real) transfer from a dynamics and controls perspective usually involves re-tuning or adapting the designed algorithms to suit real-world operating conditions, which often violates the performance guarantees established originally. This work presents a generalizable framework for achieving reliable sim2real transfer of autonomy-oriented control systems using multi-model multi-objective robust optimal control synthesis, which lends well to uncertainty handling and disturbance rejection with theoretical guarantees. Particularly, this work is centered around an actuation-redundant scaled autonomous vehicle called Nigel, with independent all-wheel drive and independent all-wheel steering architecture, whose enhanced configuration space bodes well for robust control applications. To this end, we present a systematic study on the complete mechatronic design, dynamics modeling, parameter identification, and robust stabilizing as well as steady-state tracking control of Nigel using the proposed framework, with experimental validation.

Index Terms—Autonomous vehicles, 4WD4WS vehicles, over-actuated systems, mechatronic design, robust optimal control, linear matrix inequalities, sim2real transfer, uncertainty handling, disturbance rejection.

I. INTRODUCTION

MODERN day automotive systems exploit a combination of mechanical electrical, electronic, networking, and software sub-systems to enhance performance via a hierarchical suite of autonomy-oriented control realizations. While earlier autonomy developers may have enjoyed the freedom of primarily focusing on core software development, the present context demands a paradigm shift towards a synergistic hardware-software co-design approach, harmonizing with the principles of mechatronics engineering [1]. In particular, the demand for increased maneuverability, enhanced control configuration space, and improved tolerance against faults motivates the pursuit of unconventional vehicle designs. In response, autonomous vehicle (AV) realizations must augment their underlying hardware-software architectures to enhance core performance as well as adaptability to changing operating conditions. However, with the advent of novel design architectures, advanced control strategies [2] are required to fully exploit the added capabilities. Moreover, the devised control systems need to successfully transition the sim2real

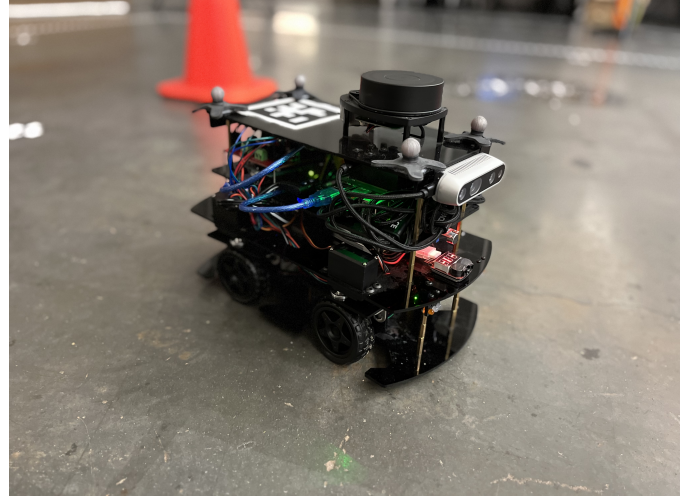


Fig. 1. Nigel: A mechatronically redundant and reconfigurable 1:14 scale autonomous vehicle. This modular and open-source vehicle platform offers multiple driving/steering configurations, abundant interoceptive/exteroceptive sensors, on-board edge-AI computation and wired/wireless communication, selectively constrained software-defined actuation, as well as a fully functional lighting and signaling system. A video highlighting key features of Nigel is available at <https://youtu.be/UVIShZuZmpg>

gap by guaranteeing robust performance against real-world uncertainties and disturbances. This further calls for model and simulation-based controller refinement along with real-world testing, which requires capable cyber-physical deployment platforms of varying scales. Previous works have tried to address some of these aspects, albeit in a fragmented sense as we will review below.

In the context of developing scaled autonomous vehicles, educational and research institutes have contributed platforms like the MIT Racecar [3], AutoRally [4], FITENTH [5], Multi-agent System for non-Holonomic Racing (MuSHR) [6], Optimal RC Racing (ORCA) Project [7], Delft Scaled Vehicle (DSV) [8] and Berkeley Autonomous Race Car (BARC) [9]. Community-driven projects such as HyphaROS Race-Car [10] and Donkey Car [11] have also emerged, which are often tailored for specific applications like map-based navigation and vision-aided imitation learning, respectively. Moreover, commercial products like Quanser QCar [12] and AWS DeepRacer [13] have also entered the market, but their closed-source nature and prohibitive costs limit their accessibility to the broader community. Additionally, scaled robot platforms like the TurtleBot3 [14] and Duckiebot [15] remain valuable for teaching fundamental autonomy concepts. However, none of the aforementioned platforms (refer Table I)

*These authors contributed equally.

C. V. Samak, T. V. Samak and V. N. Krovi are with the Automation, Robotics and Mechatronics Laboratory (ARMLab), Department of Automotive Engineering, Clemson University International Center for Automotive Research (CU-ICAR), Greenville, SC 29607, USA. Email: {csamak, tsamak, vkrovi}@clemson.edu

J. M. Velni is with the Velni Lab, Department of Mechanical Engineering, Clemson University, Clemson, SC 29634, USA. Email: javadm@clemson.edu

TABLE I
COMPARATIVE ANALYSIS OF POPULAR SCALED AUTONOMOUS VEHICLE PLATFORMS

Platform	Cost [†]	Sensing Modalities								Computational Resources			Actuation Mechanism [‡]	Lights & Indicators	V2X Support	API Support									
	Scale	Open Hardware	Open Software	Throttle	Steering	Wheel Encoders	GPS/IMU	IMU	Microphone	LIDAR	Monocular Camera	Depth/Stereo Camera	High-Level	Low-Level	Lights	Buzzer/Speaker	V2V	V2I	C++	Python	ROS	ROS 2	Autaware	MATLAB/Simulink	Webapp
Nigel (Ours)	1:14	✓	✓	\$600	✓	✓	✓	✓	✓	✓	✓	✓	Jetson Orin Nano	Arduino Mega	4WD4WS	✓	✓	✓	✓	✓	✓	✓	✓	✓	✓
MIT Racecar	1:10	★	✓	\$2,600	✗	✗	✗	✓	✗	✗	✗	✗	Jetson TX2	VESC	AS	✗	✗	✗	★	✗	✗	✗	✗	✗	✗
AutoRally	1:5	★	✓	\$23,300	✗	✗	✓	✓	✓	✓	✓	✓	Custom	Teensy LC/Arduino Micro	AS	✗	✗	✗	★	✗	✗	✗	✗	✗	✗
FITENTH	1:10	★	✓	\$3,260	✗	✗	✗	✗	✗	✗	✗	✗	Jetson TX2	VESC 6Mkv	AS	✗	✗	✓	✗	✗	✗	✗	✓	✗	✗
DSV	1:10	★	✓	\$1,000	✗	✗	✓	✓	✓	✓	✓	✓	ODROID-XU4	Arduino (Mega + Uno)	AS	✗	✗	✗	✗	✗	✓	✓	✗	✗	✗
MuSHR	1:10	★	✓	\$930	✗	✗	✓	✓	✓	✓	✓	✓	Jetson Nano	Turnigy SK8-ESC	AS	✗	✗	✓	✗	✗	✗	✗	✗	✗	✗
BARC	1:10	★	✓	\$1,030	✗	✗	✓	✓	✓	✓	✓	✓	ODROID-XU4	Arduino Nano	AS	✗	✗	✗	✗	✗	✗	✗	✗	✗	✗
ORCA	1:43	✓	✓	\$960	✗	✗	✗	✗	✗	✗	✗	✗	None	ARM Cortex M4 µC	AS	✗	✗	✓	✓	✗	✗	✗	✗	✗	✗
HyphaROS	1:10	★	✓	\$600	✗	✗	✓	✓	✓	✓	✓	✓	ODROID-XU4	RC ESC TBLE-02S	AS	✗	✗	✗	✗	✗	✗	✗	✗	✗	✗
Donkey Car	1:16	★	✓	\$370	✗	✗	✗	✗	✗	✗	✗	✗	Raspberry Pi	ESC	AS	✗	✗	✗	✗	✗	✗	✗	✗	✗	✗
QCcar	1:10	✗	✗	\$20,000	✗	✗	✓	✓	✓	✓	✓	✓	Jetson TX2	Proprietary	AS	✓	✓	✓	✗	★	★	✗	✗	✓	✗
DeepRacer	1:18	✗	✗	\$400	✗	✗	✗	✓	✗	✗	✗	✗	Proprietary	Proprietary	AS	✗	✗	✗	✗	✗	✗	✗	✗	✗	✓
Duckiebot	N/A	✓	✓	\$450	✗	✗	✗	✗	★	✗	✗	✗	Raspberry Pi/Jetson Nano	None	DD	★	★	★	✗	✗	✓	✗	✗	✗	✗
TurtleBot3	N/A	✓	✓	\$590	✗	✗	✓	✓	✓	✓	✓	✓	Raspberry Pi	OpenCR	DD	✗	✗	★	✗	✗	✓	✗	★	✗	✗

[†]All cost values are ceiled to the nearest \$10. [‡]Actuation mechanisms comprise Ackermann steered (AS), differential-drive (DD), and 4-wheel drive 4-wheel steer (4WD4WS) configurations.

✓ indicates complete fulfillment; ★ indicates conditional, unsupported or partial fulfillment; and ✗ indicates non-fulfillment.

contributes primarily towards novel vehicular configuration or architecture. Other works such as [16] and [17] have recently prototyped over-actuated scaled vehicles with the primary aim of validating their control algorithms, and as such, none of these platforms are open-sourced. Additionally, both of these platforms lack comprehensive autonomy features and only the latter offers truly independent driving and steering capability, although at a much larger scale (1:5) and without extended steering limits. To the best of authors' knowledge, Nigel (refer Fig. 1) is the first open-source¹ mechatronically redundant [18] autonomous vehicle platform offering comprehensive autonomy features as well as independent all-wheel driving and independent all-wheel steering (i.e., independent 4WD4WS) configuration with extended ($\pm 90^\circ$) steering angles, within a small footprint of 1:14 scale. Additionally, Nigel is a part of the larger AutoDRIVE Ecosystem² [19], [20], which also offers a high-fidelity digital-twin simulation platform [21], [22], as well as flexible application programming interfaces (APIs) to develop low and high-level autonomy algorithms.

In terms of developing control strategies for vehicles with unconventional architectures, prior research endeavors have proposed and applied techniques such as inverse dynamics control [23], coordinated motion control [24], adaptive steering control [25] and model predictive control [26], [27] for achieving driver-assistance as well as automatic control objectives. Although some of these works discuss the adaptability and robustness of the designed controllers in simulated experiments, they cannot guarantee similar performance in real-world conditions. Other recent works such as [28] and [29] have applied cascaded feedforward control and robust H_∞ control, respectively, to handle environmental uncertainties and disturbances using over-actuated vehicle architectures. These robust control techniques in themselves are not completely novel, and have been studied and applied to automotive systems previously for yaw-plane [30]–[32], roll-plane [33] or vertical dynamics stabilization [34], automatic emergency braking [35], trajectory tracking [36], etc.

Our work poses the problem of robust control from a “sim2real transfer” lens, to develop a generalizable framework for reliably bridging the dynamics interface of the sim2real gap. To this end, we demonstrate robust stabilizing as well as steady-state tracking control of Nigel with seamless sim2real transfer, by designing a multi-model multi-objective full-state feedback controller using a linear matrix inequality (LMI) approach, which seeks the optimal tradeoff between H_2 and H_∞ performance with D -stability. It is to be noted that, contrary to some of our previous works, which have targeted bridging the sim2real gap by increasing simulation fidelity [37], this work intentionally widens the reality gap by using a simplified linear dynamics model with lumped wheel representation to synthesize the robust optimal controller, which is hypothesized to bridge the dynamics gap during real-world deployment. As such, the devised controller is tested rigorously in simulation as well as real-world settings for different benchmark maneuvers under varying grades of disturbances and uncertainties. In addition to validating the sim2real transfer, we also analyze the controller performance against deliberately injected exogenous disturbances and uncertainties during real-world experiments. The key contributions of this paper are summarized below:

- Open-hardware, open-software design architecture of a novel 1:14 scale independent 4WD4WS autonomous vehicle, with extended steering limits is presented.
- Non-linear dynamics model of such a 4WD4WS vehicle is derived and transformed into a linear uncertain system model with reasonable parameter identification.
- Robust sim2real control framework is established and validated using exhaustive experiments in simulation as well as real-world settings.

The remainder of this paper is organized as follows. Section II elucidates the complete mechatronic design architecture of Nigel. A detailed derivation of the independent 4WD4WS vehicle dynamics model and its analysis is discussed in Section III. Formulation of the proposed generalizable robust optimal sim2real control framework is presented in Section IV. Details pertaining to its performance evaluation in simulation as well as real-world settings are discussed in Section V. Finally, Section VI presents concluding remarks and future directions.

¹Github: <https://github.com/AutoDRIVE-Ecosystem>

²Website: <https://autodrive-ecosystem.github.io>

II. VEHICLE DESIGN ARCHITECTURE

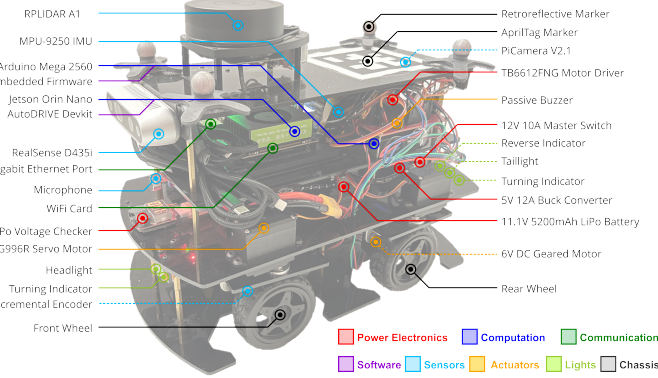


Fig. 2. Various components and sub-systems of Nigel. Dashed lines indicate occluded or hidden components.

The key design objective for vehicle architecture discussed in this work was to develop a mechatronically redundant scaled autonomous vehicle. The resulting prototype, Nigel, offers redundant driving and steering actuation, a comprehensive sensor suite, high-performance computational resources, and a standard vehicular signaling system (refer Fig. 2).

Chassis: Nigel is a 1:14 scale autonomous vehicle comprising four modular platforms, each housing distinct components of the vehicle. It offers mechatronic redundancy via comprehensive autonomy features as well as an independent 4WD4WS configuration (refer Fig. 3).

Power Electronics: Nigel is powered using an 11.1 V 5200 mAh lithium-polymer (LiPo) battery, whose health is monitored by a voltage checker. Other components such as the master switch, buck converter and motor drivers help route the power to appropriate sub-systems of the vehicle.

Sensor Suite: Nigel hosts a comprehensive sensor suite comprising throttle/steering feedbacks and 1920 CPR incremental encoders for all 4 wheels, a microphone, a 3-axis indoor-positioning system (IPS) using retroreflective/fiducial markers, a 9-axis inertial measurement unit (IMU) with raw/filtered measurements, multiple RGB/RGB-D/stereo camera(s) in the front/rear, and a 360° FOV planar LIDAR.

Computation, Communication and Software: Nigel adopts Jetson Orin Nano Developer Kit for most of its high-level computation (autonomy algorithms) and communication (V2V and V2I). Additionally, it also hosts an Arduino Mega (running the vehicle firmware) for acquiring and filtering raw sensor data, and controlling the actuators/lights/indicators.

Actuators: Nigel is actuated using four 6V 160 RPM rated 120:1 DC geared motors to drive its wheels, and four 9.4 kgf.cm servo motors to steer them; the steering actuators are saturated at $\pm 90^\circ$ w.r.t. zero-steer value. All the actuators are operated at 5V, which translates to a maximum speed of ~ 130 RPM for driving and ~ 0.19 s/60° for steering. The steering actuators are positioned directly above the respective tire contact patch, which enables zero camber gain or scrubbing while steering the wheels and keeps the actuator effort stable.

Lights and Indicators: Nigel's lighting system comprises dual-mode headlights, triple-mode turning indicators, and automated taillights with reverse indicators. Additionally, Nigel is also provided with a buzzer to allow acoustic indication.

Kinematic analysis of Nigel's configuration reveals that it has $\delta_M = \delta_m + \delta_s = 1+2 = 3$ degrees of maneuverability; this is superior among all passively stable configurations possible. Elucidation follows. Considering the vehicle's configuration space $\mathcal{C} \in \mathbb{R}^m$, the n -dimensional admissible velocity space, which is a sub-space of the generalized velocity space $\mathcal{V} \in \mathbb{R}^m$ (composed of the time derivatives of the generalized coordinates of \mathcal{C}), governs the vehicle's differential degrees of freedom (a.k.a. degree of mobility, $\delta_m = n$). Given the sliding constraint matrix $\mathbf{C}_1(\delta_i) = \begin{bmatrix} \mathbf{C}_{1f} \\ \mathbf{C}_{1s}(\delta_i) \end{bmatrix}$ for fixed (f) and steerable (s) wheels, this translates to δ_m being the dimension of the right null space of $\mathbf{C}_1(\delta_i)$, i.e., $\delta_m = \dim N[\mathbf{C}_1(\delta_i)] = 3 - \text{rank}[\mathbf{C}_1(\delta_i)]$. The degree of steerability, δ_s , is governed by the sliding constraints imposed by the i steerable wheels, with $\delta_s = \text{rank}[\mathbf{C}_{1s}(\delta_i)]; 0 \leq \delta_s \leq 2$.

Lastly, it is worth mentioning that Nigel supports modular open system architecture (MOSA) standards. This allows the users to adopt and adapt the vehicle for their custom use cases by adding, removing or replacing selective components, or extensively modifying various aspects of the vehicle design.

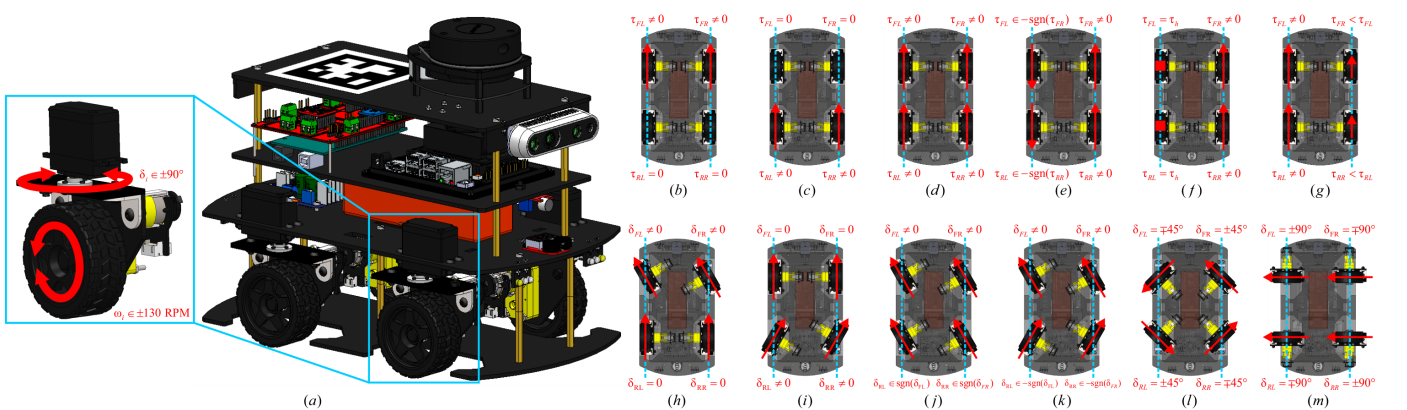


Fig. 3. Independent 4WD4WS architecture of Nigel: (a) denotes 2-DOF actuation redundancy per wheel; (b)-(g) depict common drive configurations including front-wheel drive, rear-wheel drive, all-wheel drive, neutral-steer drive, pivot-steer drive and torque vectoring drive; and (h)-(m) depict common steering configurations including front-wheel steer, rear-wheel steer, all-wheel in-phase steer, all-wheel out-of-phase steer, oblique steer and crab-walk steer.

III. DYNAMICS MODELING AND ANALYSIS

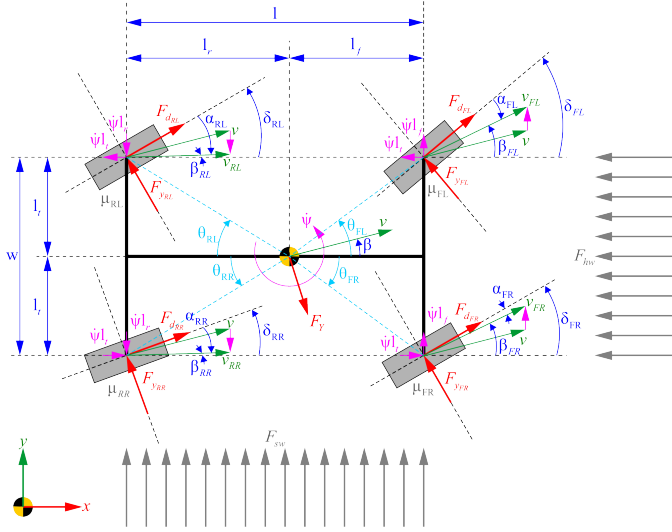


Fig. 4. Vehicle dynamics model for an independent 4WD4WS vehicle.

Considering the notations presented in Fig. 4, and following the seminal works [38], [39], we can deduce the nonlinear yaw-plane vehicle dynamics model for an independent 4WD4WS configuration as depicted in Eq. 1a-1c.

$$\begin{aligned} \sum \mathbf{F}_x : m (\dot{v} \cos(\beta) - v \dot{\beta} \sin(\beta) - \dot{\psi} v \sin(\beta)) = & \left[\frac{\tau_{RL}}{r_{RL}} \cos(\delta_{RL}) + \frac{\tau_{RR}}{r_{RR}} \cos(\delta_{RR}) \right. \\ & + \left. \frac{\tau_{FL}}{r_{FL}} \cos(\delta_{FL}) + \frac{\tau_{FR}}{r_{FR}} \cos(\delta_{FR}) \right] - \{\mu_{RL} C_{RL} [\delta_{RL} - \tan^{-1} \left(\frac{\dot{y} - \dot{\psi} l_r}{\dot{x} - \dot{\psi} l_t} \right)] \sin(\delta_{RL}) + \mu_{RR} C_{RR} [\delta_{RR} - \tan^{-1} \left(\frac{\dot{y} - \dot{\psi} l_r}{\dot{x} + \dot{\psi} l_t} \right)] \sin(\delta_{RR}) + \mu_{FL} C_{FL} [\delta_{FL} - \tan^{-1} \left(\frac{\dot{y} + \dot{\psi} l_f}{\dot{x} - \dot{\psi} l_t} \right)] \sin(\delta_{FL}) + \mu_{FR} C_{FR} [\delta_{FR} - \tan^{-1} \left(\frac{\dot{y} + \dot{\psi} l_f}{\dot{x} + \dot{\psi} l_t} \right)] \sin(\delta_{FR}) \} - F_{hw} \end{aligned} \quad (1a)$$

$$\begin{aligned} \sum \mathbf{F}_y : m (\dot{v} \sin(\beta) + v \dot{\beta} \cos(\beta) + \dot{\psi} v \cos(\beta)) = & \left[\frac{\tau_{RL}}{r_{RL}} \sin(\delta_{RL}) + \frac{\tau_{RR}}{r_{RR}} \sin(\delta_{RR}) \right. \\ & + \left. \frac{\tau_{FL}}{r_{FL}} \sin(\delta_{FL}) + \frac{\tau_{FR}}{r_{FR}} \sin(\delta_{FR}) \right] + \{\mu_{RL} C_{RL} [\delta_{RL} - \tan^{-1} \left(\frac{\dot{y} - \dot{\psi} l_r}{\dot{x} - \dot{\psi} l_t} \right)] \cos(\delta_{RL}) + \mu_{RR} C_{RR} [\delta_{RR} - \tan^{-1} \left(\frac{\dot{y} - \dot{\psi} l_r}{\dot{x} + \dot{\psi} l_t} \right)] \cos(\delta_{RR}) + \mu_{FL} C_{FL} [\delta_{FL} - \tan^{-1} \left(\frac{\dot{y} + \dot{\psi} l_f}{\dot{x} - \dot{\psi} l_t} \right)] \cos(\delta_{FL}) + \mu_{FR} C_{FR} [\delta_{FR} - \tan^{-1} \left(\frac{\dot{y} + \dot{\psi} l_f}{\dot{x} + \dot{\psi} l_t} \right)] \cos(\delta_{FR}) \} + F_{sw} \end{aligned} \quad (1b)$$

$$\begin{aligned} \sum \mathbf{M}_z : I_z \ddot{\psi} = l_f \left\{ -\frac{\tau_{FL}}{r_{FL}} \sin(\delta_{FL} - \theta_{FL}) + \frac{\tau_{FR}}{r_{FR}} \sin(\delta_{FR} + \theta_{FR}) + \mu_{FL} C_{FL} [\delta_{FL} - \tan^{-1} \left(\frac{\dot{y} + \dot{\psi} l_f}{\dot{x} - \dot{\psi} l_t} \right)] \cos(\delta_{FL} - \theta_{FL}) + \mu_{FR} C_{FR} [\delta_{FR} - \tan^{-1} \left(\frac{\dot{y} + \dot{\psi} l_f}{\dot{x} + \dot{\psi} l_t} \right)] \cos(\delta_{FR} + \theta_{FR}) \right\} - l_r \left\{ \frac{\tau_{RL}}{r_{RL}} \sin(\delta_{RL} + \theta_{RL}) - \frac{\tau_{RR}}{r_{RR}} \sin(\theta_{RR} - \delta_{RR}) + \mu_{RL} C_{RL} [\delta_{RL} - \tan^{-1} \left(\frac{\dot{y} - \dot{\psi} l_r}{\dot{x} - \dot{\psi} l_t} \right)] \cos(\delta_{RL} + \theta_{RL}) + \mu_{RR} C_{RR} [\delta_{RR} - \tan^{-1} \left(\frac{\dot{y} - \dot{\psi} l_r}{\dot{x} + \dot{\psi} l_t} \right)] \cos(\theta_{RR} - \delta_{RR}) \right\} + \left(\frac{l_f - l_r}{2} \right) F_{sw} \end{aligned} \quad (1c)$$

where, $F_{y_i} = \mu_i C_i \alpha_i$ and $F_{d_i} = \begin{cases} \tau_i / r_i; & \text{if } \tau_i / r_i \leq \mu_i N_i \\ \mu_i N_i; & \text{otherwise} \end{cases}$ are tire forces and drive forces for i -th wheel, respectively. The tire slip angle $\alpha_i = \delta_i - \beta_i$, where $\beta_i = \tan^{-1} \left(\frac{\dot{y} \pm \dot{\psi} l_f / r}{\dot{x} \pm \dot{\psi} l_t} \right)$.

TABLE II
MEASURED AND IDENTIFIED PARAMETERS OF NIGEL

Parameter	Symbol	Value	Unit
<i>Measured Parameters</i>			
Mass	m	2.68	kg
Dimensions ($L \times B \times H$)	—	$0.31847 \times 0.175 \times 0.2568$	m
Wheelbase	l	0.14155	m
Track width	l_t	0.14724	m
Wheel radius	r_i	0.0325	m
<i>Identified Parameters</i>			
Yaw moment of inertia	I_z	0.01944	$\text{kg} \cdot \text{m}^2$
CG front offset	l_f	0.06226	m
CG rear offset	l_r	0.07929	m
Friction coefficient (nominal)	μ_i	0.4	—
Tire stiffness	C_i	22.4768	$\text{N} \cdot \text{rad}^{-1}$

This model can be linearized by applying the small-angle approximation so that $\sin(\odot) \approx \odot$, $\cos(\odot) \approx 1$ and $\tan^{-1}(\odot) \approx \odot$. Additionally, we assume that the vehicle is driving at a constant velocity, implying $\dot{v} \approx 0 \Rightarrow \tau_i \approx 0$. Finally, it is also assumed that $\dot{x} \gg \dot{\psi} l_t \Rightarrow \dot{x} \pm \dot{\psi} l_t \approx \dot{x}$. Also note that F_{sw} is hereafter referred to as F_w for simplicity, since F_{hw} does not affect the linearized model.

$$\begin{bmatrix} \dot{\beta} \\ \dot{\psi} \end{bmatrix} = \begin{bmatrix} a_{11} & a_{12} \\ a_{21} & a_{22} \end{bmatrix} \begin{bmatrix} \beta \\ \psi \end{bmatrix} + \begin{bmatrix} b_{11} & b_{12} & b_{13} & b_{14} \\ b_{21} & b_{22} & b_{23} & b_{24} \end{bmatrix} \begin{bmatrix} \delta_{FL} \\ \delta_{FR} \\ \delta_{RL} \\ \delta_{RR} \end{bmatrix} + \begin{bmatrix} d_1 \\ d_2 \end{bmatrix} F_w \quad (2)$$

where,

$$\begin{aligned} a_{11} &= \frac{-1}{mv} (\mu_{FL} C_{FL} + \mu_{FR} C_{FR} + \mu_{RL} C_{RL} + \mu_{RR} C_{RR}) \\ a_{12} &= \left\{ \frac{1}{mv^2} [l_r (\mu_{RL} C_{RL} + \mu_{RR} C_{RR}) - l_f (\mu_{FL} C_{FL} + \mu_{FR} C_{FR})] \right\} - 1 \\ a_{21} &= \frac{1}{I_z} [l_r (\mu_{RL} C_{RL} + \mu_{RR} C_{RR}) - l_f (\mu_{FL} C_{FL} + \mu_{FR} C_{FR})] \\ a_{22} &= \frac{-1}{I_z v} [l_f^2 (\mu_{FL} C_{FL} + \mu_{FR} C_{FR}) + l_r^2 (\mu_{RL} C_{RL} + \mu_{RR} C_{RR})] \\ b_{11} &= \frac{\mu_{FL} C_{FL}}{mv} \quad b_{21} = \frac{l_f \mu_{FL} C_{FL}}{I_z} \quad b_{12} = \frac{\mu_{FR} C_{FR}}{mv} \\ b_{22} &= \frac{l_f \mu_{FR} C_{FR}}{I_z} \quad b_{13} = \frac{\mu_{RL} C_{RL}}{mv} \quad b_{23} = \frac{-l_r \mu_{RL} C_{RL}}{I_z} \\ b_{14} &= \frac{\mu_{RR} C_{RR}}{mv} \quad b_{24} = \frac{-l_r \mu_{RR} C_{RR}}{I_z} \quad d_1 = \frac{1}{mv} \quad d_2 = \frac{l_f - l_r}{2} \end{aligned}$$

We analyzed the model obtained in Eq. 2 based on the parameters identified (refer Table II) from lab experiments. The system has a stable equilibrium point under nominal conditions (ref Fig. 5(a)), however, drastic variation in friction or velocity significantly affects the system's damping ratio, ζ (refer Fig. 5(b)). This follows that the system is prone to face sim2real transfer issues if the environmental conditions (μ_i) are different from those in simulation or are uncertain in general, even at a constant velocity (v).

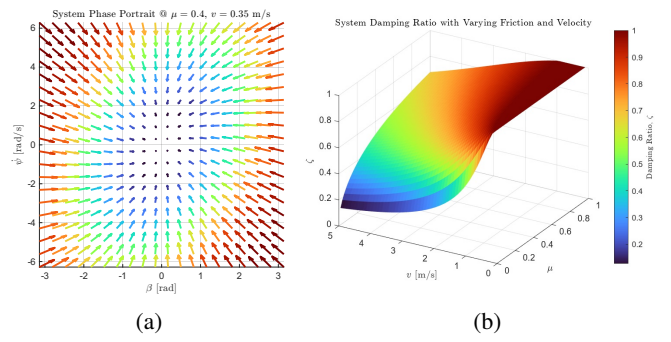


Fig. 5. Analysis of vehicle dynamics model: (a) system phase portrait; and (b) system damping ratio as a function of friction and velocity.

IV. ROBUST SIM2REAL CONTROL FRAMEWORK

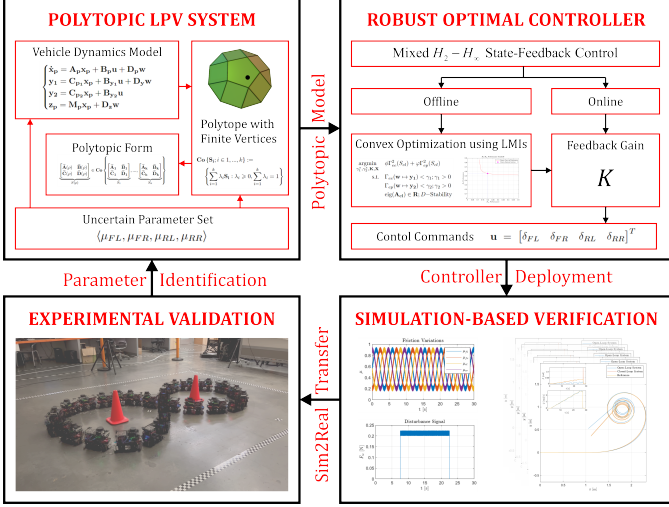


Fig. 6. Structure of the presented robust sim2real control framework.

Based on the linearized vehicle dynamics model derived in Section III a generalized representation of the open-loop system S_{ol} is formulated (refer Eq. 3).

$$S_{ol} := \begin{cases} \dot{\mathbf{x}}_p = \mathbf{A}_p \mathbf{x}_p + \mathbf{B}_p \mathbf{u} + \mathbf{D}_p \mathbf{w} \\ \mathbf{y}_1 = \mathbf{C}_{p1} \mathbf{x}_p + \mathbf{B}_{y1} \mathbf{u} + \mathbf{D}_y \mathbf{w} \\ \mathbf{y}_2 = \mathbf{C}_{p2} \mathbf{x}_p + \mathbf{B}_{y2} \mathbf{u} \\ \mathbf{z}_p = \mathbf{M}_p \mathbf{x}_p + \mathbf{D}_z \mathbf{w} \end{cases} \quad (3)$$

Here, $\mathbf{x}_p = [\beta \ \psi]^T$ are states, $\mathbf{u} = [\delta_{FL} \ \delta_{FR} \ \delta_{RL} \ \delta_{RR}]^T$ are control inputs and $\mathbf{w} = F_w$ is exogenous disturbance. The state transition is governed by $\mathbf{A}_p = \begin{bmatrix} a_{11} & a_{12} \\ a_{21} & a_{22} \end{bmatrix}$, $\mathbf{B}_p = \begin{bmatrix} b_{11} & b_{12} & b_{13} & b_{14} \\ b_{21} & b_{22} & b_{23} & b_{24} \end{bmatrix}$ and $\mathbf{D}_p = \begin{bmatrix} d_1 \\ d_2 \end{bmatrix}$. System outputs $\mathbf{y}_1 = \mathbf{y}_2 = [\mathbf{x}_p \ \mathbf{u}]^T$ are governed by $\mathbf{C}_{p1} = \mathbf{C}_{p2} = \begin{bmatrix} \mathbf{I}_{2 \times 2} \\ \mathbf{0}_{4 \times 2} \end{bmatrix}$, $\mathbf{B}_{y1} = \mathbf{B}_{y2} = \begin{bmatrix} \mathbf{0}_{2 \times 4} \\ \mathbf{I}_{4 \times 4} \end{bmatrix}$ and $\mathbf{D}_y = \mathbf{0}_{6 \times 1}$. The measurements comprise full-state feedback with $\mathbf{M}_p = \mathbf{I}_{2 \times 2}$ and $\mathbf{D}_z = \mathbf{0}_{2 \times 1}$.

Considering the sim2real gap in terms of uncertainties in frictional coefficients of the 4 road-tire interconnects $\rho = \langle \mu_{FL}, \mu_{FR}, \mu_{RL}, \mu_{RR} \rangle$, where parameters ρ_i can be time-varying or constant but uncertain, this work adopts polytopic modeling method for uncertainty treatment (refer Fig. 6). To this end, a polytopic linear parameter-varying system can be established (refer Eq. 4), where the state-space matrices depend affinely on the uncertain parameters.

$$\begin{aligned} \mathbf{A}_p(\rho) &= \mathbf{A}_0 + \mu_{FL}\mathbf{A}_1 + \mu_{FR}\mathbf{A}_2 + \mu_{RL}\mathbf{A}_3 + \mu_{RR}\mathbf{A}_4 \\ \mathbf{B}_p(\rho) &= \mathbf{B}_0 + \mu_{FL}\mathbf{B}_1 + \mu_{FR}\mathbf{B}_2 + \mu_{RL}\mathbf{B}_3 + \mu_{RR}\mathbf{B}_4 \end{aligned} \quad (4)$$

Definition 1: A polytope of $\mathbf{S}_1, \mathbf{S}_2, \dots, \mathbf{S}_k$ “vertex” systems could be represented as the convex hull of a fixed number of matrices \mathbf{S}_i with the same dimension [40], i.e.,

$$\text{Co} \{ \mathbf{S}_i; i \in 1, \dots, k \} := \left\{ \sum_{i=1}^k \lambda_i \mathbf{S}_i : \lambda_i \geq 0, \sum_{i=1}^k \lambda_i = 1 \right\} \quad (5)$$

The uncertain frictional coefficients are pragmatically assumed to be bounded with $\mu_j \in [0.1, 1.0]$ and range over a fixed polytope (refer Eq. 5) with $k = 1, 2, \dots, 16$ vertices corresponding to the 2^4 combinations of extremal parameter values, thereby encompassing all possible values of the uncertain parameters. The resulting polytopic state-space model can be written by lumping Eq. 3 to obtain Eq. 6, where $\bar{\mathbf{A}} = \mathbf{A}_p$, $\bar{\mathbf{B}} = [\mathbf{D}_p \ \mathbf{B}_p]$, $\bar{\mathbf{C}} = \begin{bmatrix} \mathbf{C}_{p1} \\ \mathbf{C}_{p2} \end{bmatrix}$ and $\bar{\mathbf{D}} = \begin{bmatrix} \mathbf{D}_y & \mathbf{B}_{y1} \\ \mathbf{0}_{6 \times 1} & \mathbf{B}_{y2} \end{bmatrix}$.

$$\begin{bmatrix} \bar{\mathbf{A}}(\rho) & \bar{\mathbf{B}}(\rho) \\ \bar{\mathbf{C}}(\rho) & \bar{\mathbf{D}}(\rho) \end{bmatrix} \in \text{Co} \left\{ \underbrace{\begin{bmatrix} \bar{\mathbf{A}}_1 & \bar{\mathbf{B}}_1 \\ \bar{\mathbf{C}}_1 & \bar{\mathbf{D}}_1 \end{bmatrix}}_{S_1}, \dots, \underbrace{\begin{bmatrix} \bar{\mathbf{A}}_k & \bar{\mathbf{B}}_k \\ \bar{\mathbf{C}}_k & \bar{\mathbf{D}}_k \end{bmatrix}}_{S_k} \right\} \quad (6)$$

Definition 2: A convex subset \mathbf{R} of a complex plane is called an n^{th} order LMI region if there exist a real symmetric matrix $\mathbf{L} \in \mathbb{R}^{n \times n}$ and a real matrix $\mathbf{M} \in \mathbb{R}^{n \times n}$ [41], which satisfy the LMI in z and \bar{z} as depicted in Eq. 7.

$$\mathbf{R} = \{z \in \mathbb{C} : \mathbf{L} + \mathbf{M}z + \mathbf{M}^T \bar{z} < 0\} \quad (7)$$

Lemma 1: A real matrix $\mathbf{A} \in \mathbb{R}^{n \times n}$ is D -stable, that is, all of its eigenvalues are in the LMI region \mathbf{R} defined by Eq. 7, if and only if there exists a positive-definite symmetric matrix $\mathbf{X} \in \mathbb{R}^{n \times n}$, which satisfies the LMI presented in Eq. 8.

$$\mathbf{L} \otimes \mathbf{X} + \mathbf{M} \otimes (\mathbf{AX}) + \mathbf{M}^T \otimes (\mathbf{AX})^T < 0 \quad (8)$$

We intend to place poles of the closed-loop system S_{cl} in the LMI region governed by the intersection of left half-plane with $\Re(z) < \alpha$ (i.e., α -stability), where $\alpha = -0.1$, and a conic sector centered at the origin having an inner angle of $\phi = 3\pi/4$ so as to guarantee some minimum decay rate and closed-loop damping. The LMI in Eq. 9a represents the α -stability region, while the one in Eq. 9b represents the conic sector centred at the origin with an inner angle of $\phi = 2\theta$.

$$2\alpha\mathbf{X} + \mathbf{AX} + (\mathbf{AX})^T < 0 \quad (9a)$$

$$\begin{bmatrix} a(\mathbf{AX} + (\mathbf{AX})^T) & -b(\mathbf{AX} - (\mathbf{AX})^T) \\ b(\mathbf{AX} - (\mathbf{AX})^T) & a(\mathbf{AX} + (\mathbf{AX})^T) \end{bmatrix} \quad (9b)$$

where, $0 < \theta < \frac{\pi}{2}$, $\cos(\theta) = \frac{-b}{\sqrt{a^2+b^2}}$, $\sin(\theta) = \frac{a}{\sqrt{a^2+b^2}}$

Definition 3: Energy-to-energy gain (or induced L_2 gain) is a performance measure of system’s response \mathbf{y} to disturbances \mathbf{w} , quantifying the amplification of the energy of input disturbances to the energy of the system outputs, and forms the supremum or H_∞ norm of the system with transfer matrix \mathbf{G} (i.e., largest singular value of the transfer matrix) as depicted in Eq. 10.

$$\Gamma_{ee} = \|\mathbf{G}\|_{H_\infty} = \sup_{\omega \in \mathbb{R}} \sigma_{\max}(\mathbf{G}(j\omega)) = \max_{\mathbf{w} \neq 0} \frac{\|\mathbf{y}\|_{L_2}}{\|\mathbf{w}\|_{L_2}} \quad (10)$$

Lemma 2: Considering the polytopic system presented in Eq. 6, the following statements are equivalent.

- 1) The system is stable with a quadratic H_∞ performance index γ_1
- 2) $\Gamma_{ee} < \gamma_1$

- 3) There exists a single matrix $\mathbf{P} > 0$ such that the following LMI is satisfied:

$$\begin{bmatrix} \mathbf{P}\tilde{\mathbf{A}}(\rho) + \tilde{\mathbf{A}}^T(\rho)\mathbf{P} & \mathbf{P}\tilde{\mathbf{B}}(\rho) & \tilde{\mathbf{C}}^T(\rho) \\ * & -\gamma_1\mathbf{I} & \tilde{\mathbf{D}}^T(\rho) \\ * & * & -\gamma_1\mathbf{I} \end{bmatrix} < 0 \quad (11)$$

- 4) There exists $\mathbf{P} > 0$ such that the following system of LMIs is satisfied for $i = 1, 2, \dots, k$:

$$\begin{bmatrix} \mathbf{P}\tilde{\mathbf{A}}_i + \tilde{\mathbf{A}}_i^T\mathbf{P} & \mathbf{P}\tilde{\mathbf{B}}_i & \tilde{\mathbf{C}}_i^T \\ * & -\gamma_1\mathbf{I} & \tilde{\mathbf{D}}_i^T \\ * & * & -\gamma_1\mathbf{I} \end{bmatrix} < 0 \quad (12)$$

Definition 4: Energy-to-peak gain is a measure of system's response \mathbf{y} to disturbances \mathbf{w} , quantifying the energy amplification of disturbances to their peak values as they propagate through the system to the outputs (i.e., energy of the impulse response), and forms the generalized H_2 norm of the system with transfer matrix \mathbf{G} as depicted in Eq. 13.

$$\|\mathbf{G}\|_{H_2}^2 = \frac{1}{2\pi} \int_{-\infty}^{\infty} \text{trace}[\mathbf{G}^*(j\omega)\mathbf{G}(j\omega)] d\omega$$

$$\Gamma_{ep} = \|\mathbf{G}\|_{H_2} = \max_{\mathbf{w} \neq 0} \frac{\|\mathbf{y}\|_{L_\infty}}{\|\mathbf{w}\|_{L_2}} \quad (13)$$

Lemma 3: Following statements are equivalent considering the polytopic system presented in Eq. 6.

- 1) The system is stable with a quadratic H_2 performance index γ_2
- 2) $\Gamma_{ep} < \gamma_2$
- 3) There exist $\mathbf{P} > 0$ and $\mathbf{Q} > 0$ such that the following conditions are satisfied:

$$\begin{aligned} \text{trace}[\tilde{\mathbf{C}}(\rho)\mathbf{P}\tilde{\mathbf{C}}^T(\rho)] &< \gamma_2^2 \\ \tilde{\mathbf{A}}(\rho)\mathbf{P} + \mathbf{P}\tilde{\mathbf{A}}^T(\rho) + \tilde{\mathbf{B}}(\rho)\tilde{\mathbf{B}}^T(\rho) &< 0 \\ \text{trace}[\tilde{\mathbf{B}}^T(\rho)\mathbf{Q}\tilde{\mathbf{B}}(\rho)] &< \gamma_2^2 \\ \tilde{\mathbf{A}}^T(\rho)\mathbf{Q} + \mathbf{Q}\tilde{\mathbf{A}}(\rho) + \tilde{\mathbf{C}}^T(\rho)\tilde{\mathbf{C}}(\rho) &< 0 \end{aligned} \quad (14)$$

- 4) There exist $\mathbf{P} > 0$ and $\mathbf{Q} > 0$ such that the following sets of conditions are satisfied for $i = 1, 2, \dots, k$:

$$\begin{aligned} \text{trace}[\tilde{\mathbf{C}}_i\mathbf{P}\tilde{\mathbf{C}}_i^T] &< \gamma_2^2 \\ \tilde{\mathbf{A}}_i\mathbf{P} + \mathbf{P}\tilde{\mathbf{A}}_i^T + \tilde{\mathbf{B}}_i\tilde{\mathbf{B}}_i^T &< 0 \\ \text{trace}[\tilde{\mathbf{B}}_i^T\mathbf{Q}\tilde{\mathbf{B}}_i] &< \gamma_2^2 \\ \tilde{\mathbf{A}}_i^T\mathbf{Q} + \mathbf{Q}\tilde{\mathbf{A}}_i + \tilde{\mathbf{C}}_i^T\tilde{\mathbf{C}}_i &< 0 \end{aligned} \quad (15)$$

Lemma 4: Given matrices \mathbf{L} , \mathbf{B} and \mathbf{Q} , the inequality $\mathbf{B}\mathbf{K}\mathbf{L} + \mathbf{L}^T\mathbf{K}^T\mathbf{B}^T + \mathbf{Q} < 0$ has a solution for \mathbf{K} if and only if the conditions presented in Eq. 16 are satisfied.

$$\begin{aligned} \mathbf{B}^\perp\mathbf{Q}\mathbf{B}^{\perp T} &< 0 \\ \mathbf{L}^T\mathbf{Q}\mathbf{L}^{T\perp} &< 0 \end{aligned} \quad (16)$$

It can be shown that applying Eq. 16 to Eq. 11-12, we can arrive at Eq. 17a-17d and much in the same way, by applying Eq. 16 to Eq. 14-15, we can obtain Eq. 18a-18d.

Theorem 1: For a given plant of order n_p , there exists an H_∞ controller of order $n_c \leq n_p$ to stabilize the closed-loop system and guarantees $\Gamma_{ee} < \gamma_1$ if and only if the conditions presented in Eq. 17a-17d are satisfied.

$$\begin{bmatrix} \mathbf{B}_p & \mathbf{A}_p\mathbf{X} + \mathbf{X}\mathbf{A}_p^T + \mathbf{D}_p\mathbf{D}_p^T & \mathbf{X}\mathbf{C}_{p_1}^T + \mathbf{D}_p\mathbf{D}_y^T \\ \mathbf{B}_{y_1} & * & \mathbf{D}_y\mathbf{D}_y^T - \gamma_1^2\mathbf{I} \end{bmatrix} \begin{bmatrix} \mathbf{B}_p \\ \mathbf{B}_{y_1} \end{bmatrix}^\perp \quad (17a)$$

$$\begin{bmatrix} \mathbf{M}_p^T \\ \mathbf{D}_z^T \end{bmatrix}^\perp \begin{bmatrix} \mathbf{Y}\mathbf{A}_p + \mathbf{A}_p^T\mathbf{Y} + \mathbf{C}_{p_1}^T\mathbf{C}_{p_1} & \mathbf{Y}\mathbf{D}_p + \mathbf{C}_{p_1}^T\mathbf{D}_y \\ * & \mathbf{D}_y^T\mathbf{D}_y - \gamma_1^2\mathbf{I} \end{bmatrix} \begin{bmatrix} \mathbf{M}_p^T \\ \mathbf{D}_z^T \end{bmatrix}^\perp \quad (17b)$$

$$\begin{bmatrix} \mathbf{X} & \gamma_1\mathbf{I} \\ \gamma_1\mathbf{I} & \mathbf{Y} \end{bmatrix} \geq 0 \quad (17c)$$

$$\text{rank} \begin{bmatrix} \mathbf{X} & \gamma_1\mathbf{I} \\ \gamma_1\mathbf{I} & \mathbf{Y} \end{bmatrix} \leq n_p + n_c \quad (17d)$$

Remark 1: The constraints imposed by Eq. 17a-17c are convex, whereas Eq. 17d being rank constraint, is not convex.

Remark 2: For a full-order controller, i.e., $n_c = n_p$, constraint imposed by Eq. 17d is satisfied and the resultant overall problem becomes convex.

Remark 3: For full-state feedback controller, i.e., $n_c = 0$ and $\mathbf{M}_p = \mathbf{I}$ constraints imposed by Eq. 17b-17d are satisfied and the resultant overall problem becomes convex.

Theorem 2: For a given plant of order n_p , there exists an H_2 controller of order $n_c \leq n_p$ to stabilize the closed-loop system and guarantees $\Gamma_{ep} < \gamma_2$ if and only if the conditions presented in Eq. 18a-18d are satisfied.

$$\begin{bmatrix} \mathbf{B}_p^\perp & (\mathbf{A}_p\mathbf{X} + \mathbf{X}\mathbf{A}_p^T + \mathbf{D}_p\mathbf{D}_p^T) \\ \mathbf{C}_{p_2} & \mathbf{X}\mathbf{C}_{p_2}^T < \gamma_2^2\mathbf{I} \end{bmatrix} \mathbf{B}_p^{\perp T} < 0 \quad (18a)$$

$$\begin{bmatrix} \mathbf{M}_p^T \\ \mathbf{D}_z^T \end{bmatrix}^\perp \begin{bmatrix} \mathbf{Y}\mathbf{A}_p + \mathbf{A}_p^T\mathbf{Y} & \mathbf{Y}\mathbf{D}_p \\ * & -\mathbf{I} \end{bmatrix} \begin{bmatrix} \mathbf{M}_p^T \\ \mathbf{D}_z^T \end{bmatrix}^\perp \quad (18b)$$

$$\begin{bmatrix} \mathbf{X} & \mathbf{I} \\ \mathbf{I} & \mathbf{Y} \end{bmatrix} \geq 0 \quad (18c)$$

$$\text{rank} \begin{bmatrix} \mathbf{X} & \mathbf{I} \\ \mathbf{I} & \mathbf{Y} \end{bmatrix} \leq n_p + n_c \quad (18d)$$

Remark 4: The constraints imposed by Eq. 18a-18c are convex, whereas Eq. 18d being rank constraint, is not convex.

Remark 5: For a full-order controller, i.e., $n_c = n_p$, constraint imposed by Eq. 18d is satisfied and the resultant overall problem becomes convex.

Remark 6: For full-state feedback controller, i.e., $n_c = 0$ and $\mathbf{M}_p = \mathbf{I}$ constraints imposed by Eq. 18b-18d are satisfied and the resultant overall problem becomes convex.

From the solution $\{\mathbf{X}, \mathbf{Y}\}$ to the convex optimization problem of minimizing $\text{trace}(\mathbf{X} + \mathbf{Y})$ subject to the inequalities presented in Eq. 17a and Eq. 18a, we can build the Lyapunov matrix and obtain the solution for the optimal state-feedback controller \mathbf{K} whose purpose is to minimize the influence of the disturbance \mathbf{w} on the system response $\mathbf{y} = [y_1 \ y_2]^T$ resulting in a closed-loop system S_{cl} with $\mathbf{A}_{cl} = (\mathbf{A}_p + \mathbf{B}_p\mathbf{K})$. That is to say that we obtain an optimal state-feedback control $\mathbf{u} = \mathbf{K}\mathbf{x}_p$ that:

- Places the poles of S_{cl} within the intersection of LMI regions \mathbf{R} specified by Eq. 9a and Eq. 9b.
- Bounds Γ_{ee} of S_{cl} from \mathbf{w} to \mathbf{y}_1 below $\gamma_1 > 0$.
- Bounds Γ_{ep} of S_{cl} from \mathbf{w} to \mathbf{y}_2 below $\gamma_2 > 0$.
- Minimizes the H_2-H_∞ tradeoff criterion of the form $\phi\Gamma_{ee}^2 + \varphi\Gamma_{ep}^2$ with ϕ and φ being weights on the respective performance measures.

Remark 7: With the specific choice of output quantities $\mathbf{y} = [y_1 \ y_2]^T$ as stated earlier, we can see that the designed controller penalizes deviation of state \mathbf{x}_p from zero (for stabilization) and reference \mathbf{x}_r (for tracking) along with the 4 control inputs $\mathbf{u} = [\delta_{FL} \ \delta_{FR} \ \delta_{RL} \ \delta_{RR}]^T$ so as to conserve energy by reducing the control effort.

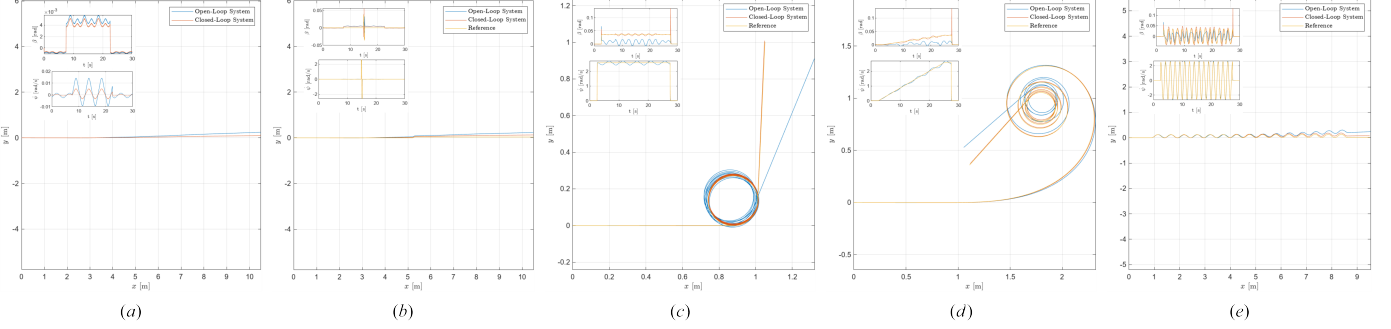


Fig. 7. The simulation experiments comprised testing the controller for (a) stabilizing as well as steady-state tracking of standard benchmark maneuvers viz. (b) lane-change, (c) skidpad, (d) fishhook and (e) slalom tests, against varying friction for individual road-tire interconnects and wind-gust disturbances.

V. RESULTS AND DISCUSSION

The closed-loop system derived in Section IV was found to be robustly stable over the entire specified parameter range, since a single Lyapunov function of the form $\mathbf{V}(\mathbf{x}_p, \alpha) = \mathbf{x}_p^T \mathbf{Q}^{-1}(\alpha) \mathbf{x}_p$, $\mathbf{Q}(\alpha) = \alpha_1 \mathbf{Q}_1 + \dots + \alpha_k \mathbf{Q}_k$ was obtained such that $\frac{d}{dt} \mathbf{V}(\mathbf{x}_p, \alpha) < 0$ for all polytopic decompositions.

We analyzed the performance of the robust optimal controller in simulation as well as real-world settings. The design of experiments followed a similar approach for both. The stabilizing controller was tested for a straight-line maneuver. For the tracking controller, reference generation was achieved by running the open-loop system with standard test signals viz. impulse, step, ramp and sine, which resulted in benchmark maneuvers viz. lane-change, skidpad, fishhook and slalom, respectively in the absence of any disturbances or parameter variations. It is worth mentioning that the controllers discussed in this work are designed to track the vehicle states, which in turn results in spatiotemporal trajectory tracking.

The simulation experiments comprised testing the controller for stabilizing as well as steady-state tracking of standard benchmark maneuvers viz. lane-change, skidpad, fishhook and slalom, against environmental uncertainties (refer Fig. 7). Particularly, the friction for individual road-tire interconnects was simulated as phase-shifted sinusoids, such that all 4 wheels never experienced the same μ , and wind-gust disturbances were simulated as delayed step input between $t=7.5$ to $t=22.5$ seconds. Apart from the results presented in this section, the

controller was tested exhaustively for varying velocities of the vehicle, with values as high as 10 times the nominal operating limit. Additionally, we also synthesized and validated a similar robust optimal controller for nominal full-scale vehicle parameters. Analysis revealed that the same design framework (refer Fig. 6) is effective for such extensions.

Upon validating the controller performance in simulation, we deployed the controller on the physical prototype of Nigel and validated its performance in a real-world experiment. The said experiment involved steady-state tracking of ‘‘Figure-8’’ maneuver, where the state feedbacks were obtained using the OptiTrack motion capture system (refer Fig. 8). In order to widen the sim2real gap, the test surface was deliberately left unclean with dust/sand particles, irregular scratches and tape residues from previous experiments. Additionally, soap-water solutions of varying concentrations were spilled in uneven quantities on the anticipated path, to induce uncertainty in terms of road friction. Finally, similar to the simulation experiments, the vehicle was disturbed actively by poking it with a pole at $t=52$, $t=68$, $t=81$ and $t=109$ seconds, which acted as an impulse input.

VI. CONCLUSION

In this work, we first introduced the complete mechatronic design architecture of Nigel and also presented the detailed dynamics modeling of this independent 4WD4WS vehicle. We also formulated a linear parameter-varying polytopic model of the system for synthesizing a robust optimal controller using an LMI approach, which seeks to minimize the H_2 - H_∞ tradeoff criteria while satisfying the closed-loop pole placement constraints in a Pareto-optimization scheme. We demonstrated and analyzed robust stabilizing as well as steady-state tracking control of Nigel with exhaustive simulation-based verification. The proposed reliable sim2real framework was also experimentally validated using the 4WD4WS vehicle platform. In addition to sim2real transfer, we also validated the controller to handle extra disturbance and uncertainties in real-world conditions.

Future work will delve into formulating and validating a robust tracking problem using mixed sensitivity loop-shaping. Other avenues include fault-tolerant control, and integration of the proposed framework with a high-level autonomy stack, by taking advantage of Nigel’s comprehensive sensor suite.

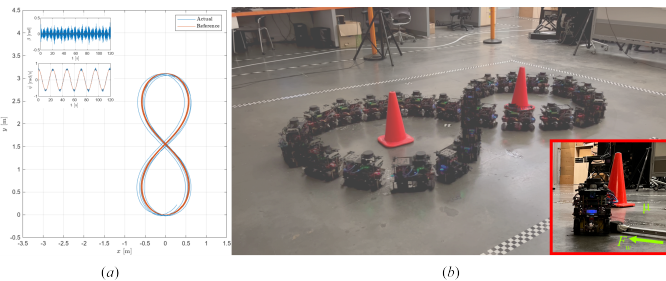


Fig. 8. The real-world experiment comprised testing the controller for steady-state tracking of a ‘‘Figure-8’’ maneuver, against varying friction for individual road-tire interconnects and poking disturbances: (a) depicts vehicle states and trajectory; and (b) visualizes the vehicle trajectory as a time-series snapshot, with the inset indicating the disturbance F_w and soap-water patches of different concentrations to vary road friction μ .

REFERENCES

- [1] C. de Silva, *Mechatronics: An Integrated Approach*. Taylor & Francis, 2004. [Online]. Available: <https://books.google.com/books?id=CjB2ygeR95cC>
- [2] C. V. Samak, T. V. Samak, and S. Kandhasamy, “Control Strategies for Autonomous Vehicles,” in *Autonomous Driving and Advanced Driver-Assistance Systems (ADAS)*. CRC Press, 2021, pp. 37–86.
- [3] S. Karaman et al., “Project-based, collaborative, algorithmic robotics for high school students: Programming self-driving race cars at MIT,” in *2017 IEEE Integrated STEM Education Conference (ISEC)*, 2017, pp. 195–203. [Online]. Available: <https://mit-racecar.github.io>
- [4] B. Goldfain, P. Drews, C. You, M. Barulic, O. Velev, P. Tsotras, and J. M. Rehg, “AutoRally: An Open Platform for Aggressive Autonomous Driving,” *IEEE Control Systems Magazine*, vol. 39, no. 1, pp. 26–55, 2019. [Online]. Available: <https://arxiv.org/abs/1806.00678>
- [5] M. O’Kelly, V. Sukhil, H. Abbas, J. Harkins, C. Kao, Y. V. Pant, R. Mangham, D. Agarwal, M. Behl, P. Burgio, and M. Bertogna, (2019) F1/10: An Open-Source Autonomous Cyber-Physical Platform. [Online]. Available: <https://arxiv.org/abs/1901.08567>
- [6] S. S. Srinivasa, P. Lancaster, J. Michalove, M. Schmittle, C. Summers, M. Rockett, J. R. Smith, S. Choudhury, C. Mavrogiannis, and F. Sadeghi. (2019) MuSHR: A Low-Cost, Open-Source Robotic Racecar for Education and Research. [Online]. Available: <https://arxiv.org/abs/1908.08031>
- [7] Automatic Control Laboratory, ETH Zürich, “ORCA (Optimal RC Racing Project),” 2021. [Online]. Available: <https://control.ee.ethz.ch/research/team-projects/autonomous-rc-car-racing.html>
- [8] T. K. et al., “Design and Development of the Delft Scaled Vehicle: A Platform for Autonomous Driving Tests,” Delft University of Technology, Delft, Netherlands, Bachelor’s Thesis, 2017. [Online]. Available: https://www.erwinrietveld.com/assets/docs/BEP11_DSCS_Paper_Final.pdf
- [9] J. Pappas, C. H. Yuan, C. S. Lu, N. Nassar, A. Miller, S. van Leeuwen, and F. Borrelli, “Berkeley Autonomous Race Car (BARC),” 2021. [Online]. Available: <https://sites.google.com/site/berkeleybarcproject>
- [10] HyphaROS Workshop, “HyphaROS Racecar,” 2021. [Online]. Available: https://github.com/Hypha-ROS/hypharos_racecar
- [11] Donkey Community, “An Open-Source DIY Self-Driving Platform for Small-Scale Cars,” 2021. [Online]. Available: <https://www.donkeycar.com>
- [12] Quanser Consulting Inc., “QCar - A Sensor-Rich Autonomous Vehicle,” 2021. [Online]. Available: <https://www.quanser.com/products/qcar>
- [13] Amazon Web Services, “AWS DeepRacer,” 2021. [Online]. Available: <https://aws.amazon.com/deepracer>
- [14] Robotis Inc., “TurtleBot3,” 2021. [Online]. Available: <https://emanual.robotis.com/docs/en/platform/turtlebot3/overview/>
- [15] L. Paull et al., “Duckietown: An Open, Inexpensive and Flexible Platform for Autonomy Education and Research,” in *2017 IEEE International Conference on Robotics and Automation (ICRA)*, 2017, pp. 1497–1504. [Online]. Available: http://michalc.net/wp-content/papercite-data/pdf/paull_2017.pdf
- [16] B. Bae and D.-H. Lee, “Design of a Four-Wheel Steering Mobile Robot Platform and Adaptive Steering Control for Manual Operation,” *Electronics*, vol. 12, no. 16, 2023. [Online]. Available: <https://www.mdpi.com/2079-9292/12/16/3511>
- [17] J. Park and Y. Park, “Multiple-Actuator Fault Isolation Using a Minimal L1-Norm Solution with Applications in Overactuated Electric Vehicles,” *Sensors*, vol. 22, no. 6, 2022. [Online]. Available: <https://www.mdpi.com/1424-8220/22/6/2144>
- [18] C. Samak, T. Samak, and V. Krovi, “Towards Mechatronics Approach of System Design, Verification and Validation for Autonomous Vehicles,” in *2023 IEEE/ASME International Conference on Advanced Intelligent Mechatronics (AIM)*, 2023, pp. 1208–1213.
- [19] T. Samak, C. Samak, S. Kandhasamy, V. Krovi, and M. Xie, “AutoDRIVE: A Comprehensive, Flexible and Integrated Digital Twin Ecosystem for Autonomous Driving Research & Education,” *Robotics*, vol. 12, no. 3, 2023. [Online]. Available: <https://www.mdpi.com/2218-6581/12/3/77>
- [20] T. V. Samak and C. V. Samak, “AutoDRIVE - Technical Report,” 2022. [Online]. Available: <https://arxiv.org/abs/2211.08475>
- [21] T. V. Samak, C. V. Samak, and M. Xie, “AutoDRIVE Simulator: A Simulator for Scaled Autonomous Vehicle Research and Education,” in *2021 2nd International Conference on Control, Robotics and Intelligent System*, ser. CCRIS’21. New York, NY, USA: Association for Computing Machinery, 2021, p. 1–5. [Online]. Available: <https://doi.org/10.1145/3483845.3483846>
- [22] T. V. Samak and C. V. Samak, “AutoDRIVE Simulator - Technical Report,” 2022. [Online]. Available: <https://arxiv.org/abs/2211.07022>
- [23] Z. Zhang, C. Yang, W. Zhang, Y. Xu, Y. Peng, and M. Chi, “Motion Control of a 4WS4WD Path-Following Vehicle: Dynamics-Based Steering and Driving Models,” *Shock and Vibration*, vol. 2021, 2021. [Online]. Available: <https://doi.org/10.1155/2021/8861159>
- [24] S. Zhu, B. Wei, D. Liu, H. Chen, X. Huang, Y. Zheng, and W. Wei, “A Dynamics Coordinated Control System for 4WD-4WS Electric Vehicles,” *Electronics*, vol. 11, no. 22, 2022. [Online]. Available: <https://www.mdpi.com/2079-9292/11/22/3731>
- [25] J. R. Kolodziej, “Adaptive Rear-Wheel Steering Control of a Four-Wheel Vehicle Over Uncertain Terrain,” ser. Dynamic Systems and Control Conference, vol. 1, 10 2012, pp. 857–866. [Online]. Available: <https://doi.org/10.1115/DSCC2012-MOVIC2012-8603>
- [26] M. Schwartz, F. Siebenrock, and S. Hohmann, “Model Predictive Control Allocation of an Over-Actuated Electric Vehicle with Single Wheel Actuators,” *IFAC-PapersOnLine*, vol. 52, no. 8, pp. 162–169, 2019, 10th IFAC Symposium on Intelligent Autonomous Vehicles IAV 2019. [Online]. Available: <https://www.sciencedirect.com/science/article/pii/S2405896319303969>
- [27] Q. Tan, P. Dai, Z. Zhang, and J. Katupitiya, “MPC and PSO Based Control Methodology for Path Tracking of 4WS4WD Vehicles,” *Applied Sciences*, vol. 8, no. 6, 2018. [Online]. Available: <https://www.mdpi.com/2076-3417/8/6/1000>
- [28] J.-E. Moseberg and G. Roppeneker, “Robust Cascade Control for the Horizontal Motion of a Vehicle with Single-Wheel Actuators,” *Vehicle System Dynamics*, vol. 53, no. 12, pp. 1742–1758, 2015. [Online]. Available: <https://doi.org/10.1080/00423114.2015.1081954>
- [29] M. Li, Y. Jia, and T. Lei, “Path Tracking of Varying-Velocity 4WS Autonomous Vehicles under Tire Force Friction Ellipse Constraints,” *Robotics and Autonomous Systems*, vol. 173, p. 104621, 2024. [Online]. Available: <https://www.sciencedirect.com/science/article/pii/S0921889024000046>
- [30] J. Ackermann and W. Sienel, “Robust Yaw Damping of Cars with Front and Rear Wheel Steering,” *IEEE Transactions on Control Systems Technology*, vol. 1, no. 1, pp. 15–20, 1993.
- [31] H. Zhang, X. Zhang, and J. Wang, “Robust Gain-Scheduling Energy-to-Peak Control of Vehicle Lateral Dynamics Stabilisation,” *Vehicle System Dynamics*, vol. 52, no. 3, pp. 309–340, 2014. [Online]. Available: <https://doi.org/10.1080/00423114.2013.879190>
- [32] S. Cheng et al., “Robust LMI-Based H-Infinity Controller Integrating AFS and DYC of Autonomous Vehicles With Parametric Uncertainties,” *IEEE Transactions on Systems, Man, and Cybernetics: Systems*, vol. 51, no. 11, pp. 6901–6910, 2021.
- [33] J. P. Redondo, B. L. Boada, and V. Díaz, “LMI-Based H-Infinity Controller of Vehicle Roll Stability Control Systems with Input and Output Delays,” *Sensors*, vol. 21, no. 23, 2021. [Online]. Available: <https://www.mdpi.com/1424-8220/21/23/7850>
- [34] A. Y. Babawuro, N. M. Tahir, M. Muhammed, and A. U. Sambo, “Optimized State Feedback Control of Quarter Car Active Suspension System Based on LMI Algorithm,” *Journal of Physics: Conference Series*, vol. 1502, no. 1, p. 012019, Mar 2020. [Online]. Available: <https://dx.doi.org/10.1088/1742-6596/1502/1/012019>
- [35] Y.-e. Mao, Y. Zheng, Y. Jing, G. M. Dimirovski, and S. Hang, “An LMI Approach to Slip Ratio Control of Vehicle Antilock Braking Systems,” in *2009 American Control Conference*, 2009, pp. 3350–3354.
- [36] M. Schwartz, T. Rudolf, and S. Hohmann, “Robust Position and Velocity Tracking Control of a Four-wheel Drive and Four-wheel Steered Electric Vehicle,” in *2020 6th International Conference on Control, Automation and Robotics (ICCAR)*, 2020, pp. 415–422.
- [37] C. Samak, T. Samak, and V. Krovi, “Towards Sim2Real Transfer of Autonomy Algorithms using AutoDRIVE Ecosystem,” *IFAC-PapersOnLine*, vol. 56, no. 3, pp. 277–282, 2023, 3rd Modeling, Estimation and Control Conference MECC 2023. [Online]. Available: <https://www.sciencedirect.com/science/article/pii/S2405896323023704>
- [38] W. Milliken and D. Milliken, *Race Car Vehicle Dynamics*, ser. Premiere Series. SAE International, 1995. [Online]. Available: <https://books.google.com/books?id=EOHPjgEACAAJ>
- [39] R. Rajamani, *Vehicle Dynamics and Control*, ser. Mechanical Engineering Series. Springer US, 2011. [Online]. Available: <https://books.google.com/books?id=q6SJcgAACAAJ>
- [40] P. Apkarian, P. Gahinet, and G. Becker, “Self-Scheduled H-Infinity Control of Linear Parameter-Varying Systems: A Design Example,” *Automatica*, vol. 31, no. 9, pp. 1251–1261, 1995. [Online]. Available: <https://www.sciencedirect.com/science/article/pii/000510989500038X>
- [41] Y. Li, “Robust Control-LMI Method,” 2002.



Chinmay Samak (Student Member, IEEE) received the B.Tech. degree in mechatronics engineering from SRM Institute of Science and Technology with a gold medal in 2021. He is currently pursuing the direct Ph.D. degree at Clemson University International Center of Automotive Research (CU-ICAR) where he is working at the ARMLab. His research interests lie at the intersection of physics-informed and data-driven methods to bridge the sim2real gap using autonomy-oriented digital twins.



Tanmay Samak (Student Member, IEEE) received the B.Tech. degree in mechatronics engineering from SRM Institute of Science and Technology with a silver medal in 2021. He is currently pursuing the direct Ph.D. degree at Clemson University International Center of Automotive Research (CU-ICAR) where he is working at the ARMLab. His research interests lie at the intersection of real and virtual worlds to bridge the real2sim gap by creating physically and graphically accurate digital twins.



Javad Velni (Senior Member, IEEE) received the Ph.D. degree in mechanical engineering from University Houston in 2008. He is a professor with the Department of Mechanical Engineering at Clemson University, where he also directs the Velni Lab. His research interests include secure control of cyber–physical systems and, in particular, transportation systems, coverage control of heterogeneous multi-agent systems, and learning-based control of complex distributed systems.



Venkat Kroví (Senior Member, IEEE) received the Ph.D. degree in mechanical engineering and applied mechanics from University of Pennsylvania in 1998. He is the Michelin Endowed Chair Professor of Vehicle Automation with the Departments of Automotive and Mechanical Engineering at Clemson University, where he also directs the ARMLab. The underlying theme of his research has been to take advantage of “power of the many” (both autonomous agents and humans) to extend the reach of human users in dull, dirty, and dangerous environments.